2026 IEEE/SICE International Symposium on System Integration (SII)
January 11-14, 2026. Cancún, México

Preliminary Demonstration of Steady-State Force Generation by High-Frequency Actuation of a High-Response Artificial Muscle Actuator Using Dimethyl Ether Combustion (HADEC)

K. Mori, K. Tsurumi, R. Sawahashi, *Member, IEEE,* and M. Okui, *Member, IEEE*

***Abstract*— This study focuses on the structure and actuation principle of biological muscles and attempts to develop a novel actuator that emulates their behavior. Pneumatic artificial muscle (PAM), particularly those of the McKibben type, have been widely utilized in assistive suits due to their lightweight design, flexibility, and high-power density. However, their reliance on compressed air results in delayed response, making them unsuitable for rapid actuation. To address this limitation, we developed a combustion-driven artificial muscle named HADEC (High-Response Artificial Muscle Actuator using Dimethyl Ether Combustion), which generates impulsive contraction force by injecting and igniting a dimethyl ether (DME)– air mixture inside the artificial muscle. Since HADEC is only capable of impulsive behavior, it has not yet been able to achieve steady-state force generation. In this study, inspired by the behavior of biological muscles, we propose and demonstrate a system in which three HADEC actuators are driven in a phase-shifted manner at a high frequency of 4.166 Hz (0.24 s cycle). Furthermore, to address the scalability issue inherent in PAMs—which require an increasing number of solenoid valves when used in multiples—we also propose a fluidic circuit architecture for HADEC that operates without the need for valves. The proposed configuration successfully achieves steady-state force generation. Experimental results show that an arm could be held within a range of 10°–20° for approximately 1.5 seconds, indicating that repeated high-frequency actuation of HADEC can emulate the behavior of biological muscles and serve as an effective approach for achieving continuous actuation.**

I. INTRODUCTION

In recent years, there has been growing interest in soft robotics [1]–[8], which aims to achieve flexible and safe motion similar to that of biological organisms. This trend has driven research and development of actuators intended for applications such as rehabilitation and physical assistance [9][10]. In these applications, actuators that combine high output with flexibility and lightweight design are required, as alternatives to rigid motors and hydraulic systems. Among such actuators, pneumatic artificial muscle (PAM) [11] has attracted significant attention as soft actuators due to their low weight, inherent safety, and high-power density. In particular, McKibben pneumatic artificial muscle [12][13], which is composed of a rubber tube and a braided sleeve, offers a simple structure that achieves high power density while maintaining flexibility and low weight, and has been employed in assistive devices and for providing haptic sensations [14][15]. However, PAM suffers from response delays due to the compressibility of air, which leads to a time lag between valve opening and actual muscle contraction. This delay hinders rapid actuation and ultimately results in a slower rise in contraction force and reduced output performance.

Many of the soft actuators proposed thus far exhibit characteristics tailored to specific applications or constraints; however, few have successfully achieved both practical force output and rapid response. For example, shape memory alloys (SMA) [16][17] can offer compactness and high-power density, but their thermal actuation results in inherently slow response times. Dielectric elastomer actuator (DEA) [18][19] is capable of millisecond-order responses, yet the force it generates is relatively low, making them unsuitable for driving heavy loads. Additionally, pneumatic systems combined with magnetorheological (MR) fluid brakes [20] can rapidly generate force by releasing stored elastic energy through instantaneous brake disengagement. However, such systems require preparatory actions and have complex mechanical structures.

To address these challenges, we have proposed a novel combustion-driven artificial muscle actuator, named HADEC (High-Response Artificial Muscle Actuator Using Dimethyl Ether Combustion), which utilizes a rapid pressure rise generated through combustion as its driving source [21]. HADEC adopts a structure similar to that of the McKibben-type artificial muscle, incorporating electrodes within the intake-side end fitting. By injecting and igniting a premixed gas of dimethyl ether (DME) and air inside the actuator chamber, HADEC instantaneously generates high pressure, resulting in contraction. This pressure rise occurs within a few milliseconds, enabling significantly faster response compared to conventional PAM. Moreover, DME, widely used as an alternative fuel to diesel, is a clean energy source that can be liquefied and stored at room temperature in aluminum containers. It produces minimal soot and particulate matter (PM) upon combustion, making it an environmentally favorable option [22]. DME also exhibits a relatively high ignition point, contributing to its safety and ease of handling. HADEC is primarily composed of a rubber tube and a braided sleeve, which allows for low-cost fabrication while maintaining the flexibility of traditional pneumatic systems and enabling high-speed impulse responses.

However, HADEC has thus far only demonstrated impulsive force generation, and the realization of continuous or steady-state force output remains an open challenge. If such steady-state force generation can be achieved, HADEC would enable a wide range of applications that require both rapid and sustained actuation. To address this limitation, the present study draws inspiration from the structure of biological muscles. Biological muscle is composed of numerous muscle fibers bundled together, each capable of

978-1-6654-5784-2/26/$31.00 ©2026 IEEE

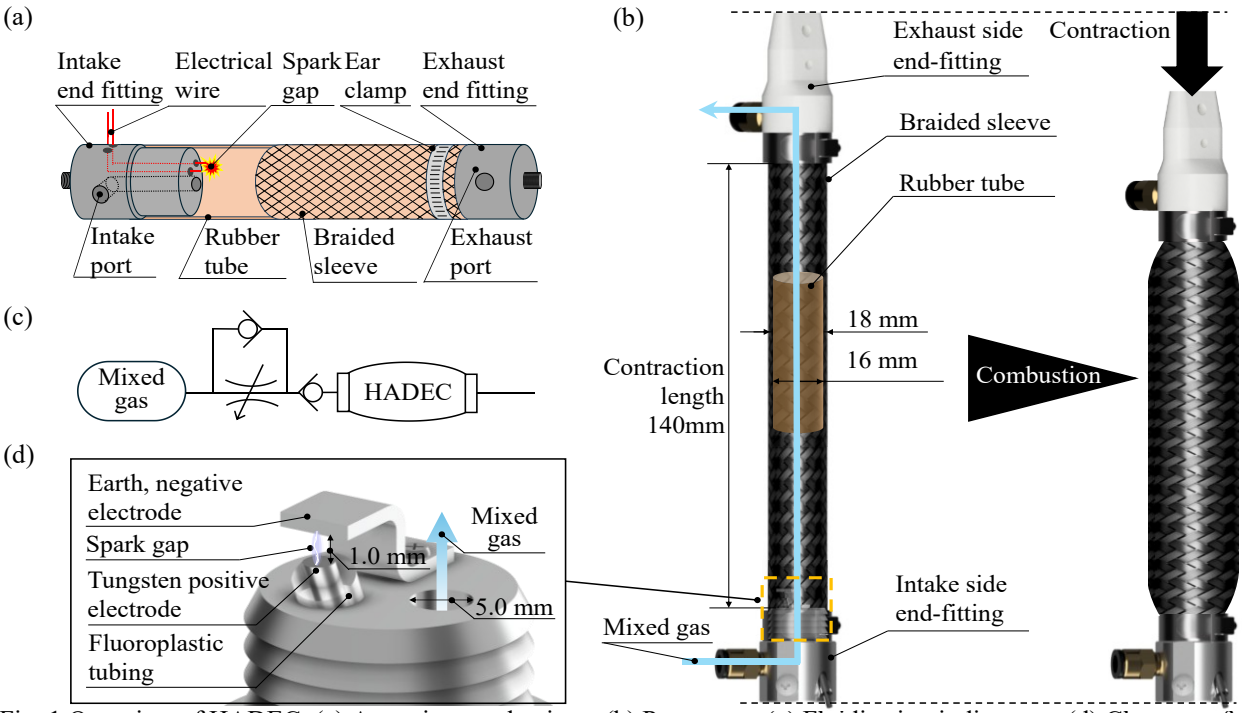

Fig. 1 Overview of HADEC: (a) Actuation mechanism. (b) Prototype. (c) Fluidic circuit diagram. (d) Close-up of electrode section.

generating impulsive contractions [23]. In biological systems, appropriate adjustment of the number of recruited muscle fibers and their contraction frequency according to the situation enables the entire muscle to achieve steady movement.

Inspired by the structural and control characteristics of biological muscles, this study investigates whether steady-state force generation can be achieved in HADEC by integrating multiple units and driving them repeatedly with phase differences—mimicking the behavior of biological muscle fibers. As a first step toward such integration, we experimentally evaluate whether three HADEC actuators, continuously supplied with fuel and driven in a repeated, phase-shifted manner, can hold an arm at a constant angle (10°–25°) for approximately 1.5 seconds. The experimental results are then compared and discussed alongside numerical simulations. Notably, unlike conventional PAM, which require an increased number of valves when scaled up, HADEC actuators generate contraction solely through ignition. Therefore, this paper also proposes a pneumatic circuit system suitable for actuator integration, in which each HADEC can be individually actuated via electrical signals using only a single shared valve.

The contributions of this study are as follows:

- We demonstrate for the first time that steady-state force generation is achievable using HADEC actuators driven impulsively at high frequencies, emulating the behavior of biological muscles.
- We propose a system architecture and actuation method suitable for the integration of multiple HADEC units, and validate their effectiveness through implementation and experimental evaluation.

II. HADEC

A. Overview

The configuration of HADEC is shown in Fig. 1(a) and (b). This artificial muscle is based on the McKibben pneumatic artificial muscle, which consists of a rubber tube enclosed in a braided sleeve. When compressed air is supplied to the interior, the actuator expands radially and contracts axially, thereby generating tensile force.

The operation of HADEC consists of the following four steps.

(1) Gas Supply: A premixed gas of DME and air is continuously supplied into the artificial muscle chamber (Fig. 1(c)).

(2) Ignition and Combustion: A high voltage is applied from an ignition coil to the electrodes embedded inside the actuator (Fig. 1(d)), generating a spark that ignites the fuel mixture.

(3) Contraction and Force Generation: The combustion causes a rapid pressure rise inside the actuator, resulting in axial contraction and the generation of driving force.

(4) Exhaust: Unreacted fuel and combustion gases are continuously expelled from the exhaust-side end fitting.

Through this process, HADEC is capable of generating high impulsive force that is difficult to achieve with conventional pneumatic actuation.

B. Dimethyl Ether (DME)

Dimethyl ether (DME, C_2H_6O) is a compound primarily synthesized via the dehydration of methanol. Its combustion yields only carbon dioxide (CO_2) and water (H_2O), resulting in low environmental impact. Consequently, DME is

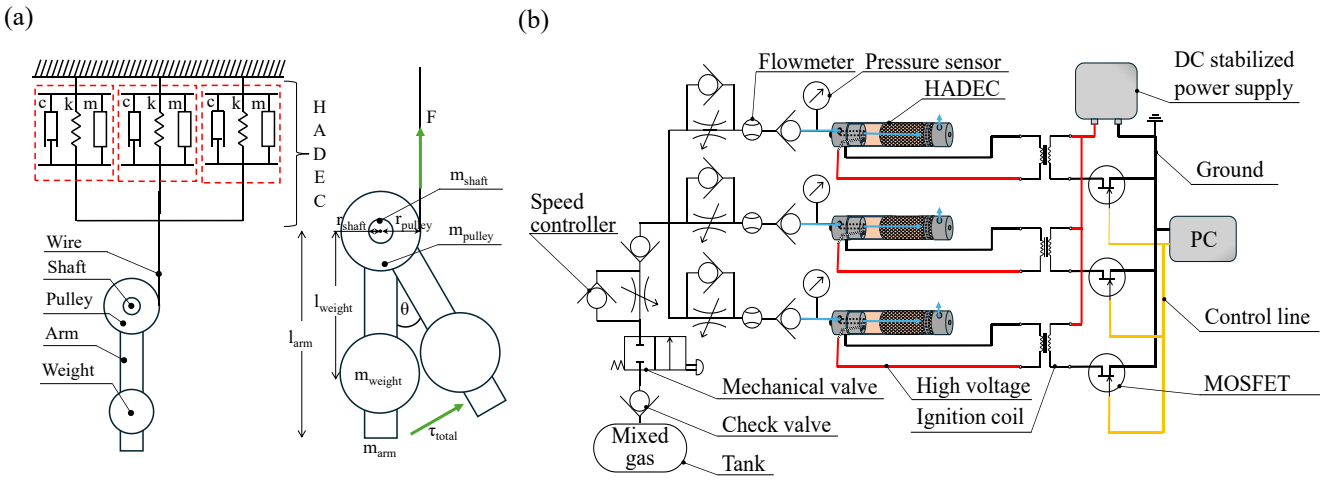

Fig. 2 (a) Schematic of the Experimental. (b) Fluidic and Electrical Circuit Diagram of the Integrated HADEC System.

considered a p romising fuel for household applications as well as for diesel engine substitution. The combustion reaction of DME is expressed as follows.

$$C_2H_6O + 3O_2 \rightarrow 2CO_2 + 3H_2O \quad (0)$$

DME is an oxygenated fuel containing oxygen within its molecular structure, which facilitates complete combustion and minimizes the emission of soot and particulate matter. In addition, it has a relatively low auto-ignition temperature of 350 °C, making it easier to ignite than methane, whose auto-ignition temperature is approximately 650 °C. DME can also be liquefied under low pressure, enabling convenient storage and transportation. Owing to these properties, it is already used in commercial products such as air dusters. These favorable characteristics make DME well suited as fuel for HADEC.

III. Integration Toward Steady-State Force Generation

A. Method for Generating Steady-State Force

To investigate whether steady-state force can be effectively generated through actuator integration, three HADEC units are arranged in parallel and driven at high frequency with phase shifts. The goal is to evaluate, through both simulation and experiment, whether such an arrangement can achieve continuous actuation of an arm via a pulley mechanism. In preliminary simulations, it was found that using only two actuators required a significantly higher driving frequency to maintain continuous force generation. However, this left insufficient time for combustion exhaust, resulting in misfires. By employing three HADEC units with appropriate phase shifts, we were able to retain a moderate actuation frequency while securing adequate exhaust intervals. For this reason, a three-actuator configuration was adopted.

The schematic of the experimental setup used in this study is shown in Fig. 2 (a). One end of each HADEC actuator is fixed, while the other end is connected to a string. This string is attached to a pulley that is rigidly coupled to a shaft. When a HADEC unit contracts, it pulls the string, thereby rotating the pulley. The pulley mechanism is employed because it allows the nonlinear yet linear-directional contraction forces of multiple HADEC actuators to be transmitted in parallel without mutual interference.

B. Modeling

In the present experiment, as illustrated in Fig. 2 (a), a string attached to the end of each HADEC actuator is wound around a pulley, which is rigidly connected to a shaft. This configuration allows the contraction of each HADEC to generate torque via the pulley. One end of the shaft is fixed to an arm, and the torque generated by the actuator causes the arm to rotate. The theoretical equations used for modeling this system are detailed in the following sections, and the corresponding parameters are summarized in Table 1 of the Appendix.

First, let the moments of inertia of the arm, weight, pulley, and shaft be denoted as I_{arm}, I_{weight}, I_{pulley}, and I_{shaft}, respectively. The total moment of inertia I_{total} is then given by.

$$I_{\text{total}} = I_{\text{arm}} + I_{\text{weight}} + I_{\text{pulley}} + I_{\text{shaft}} \quad (1)$$

Each moment of inertia is defined as follows.

$$I_{\text{arm}} = \frac{1}{12} m_{\text{arm}} \cdot {l_{\text{arm}}}^2 \quad (2)$$

$$I_{\text{weight}} = \frac{1}{2} m_{\text{weight}} \cdot {r_{\text{weight}}}^2 + m_{\text{weight}} \cdot {l_{\text{weight}}}^2 \quad (3)$$

$$I_{\text{pulley}} = \frac{1}{2} m_{\text{pulley}} \cdot \left({r_{\text{shaft}}}^2 + {r_{\text{pulley}}}^2\right) \quad (4)$$

$$I_{\text{shaft}} = \frac{1}{2} m_{\text{shaft}} \cdot {r_{\text{shaft}}}^2 \quad (5)$$

The angular acceleration of the arm, $\alpha(t) = \ddot{\theta}(t)$, is determined by the sum of the torques generated by the artificial muscle, the weight, gravity, friction, and viscous resistance.

$$I_{\text{total}} \cdot \ddot{\theta}(t) = \tau_{\text{total}}(t) = \tau_{\text{F}}(t) + \tau_{\text{weight}}(t) + \tau_{\text{gravity}}(t) + \tau_{\text{viscosity}}(t) + \tau_{\text{friction}}(t) \quad (6)$$

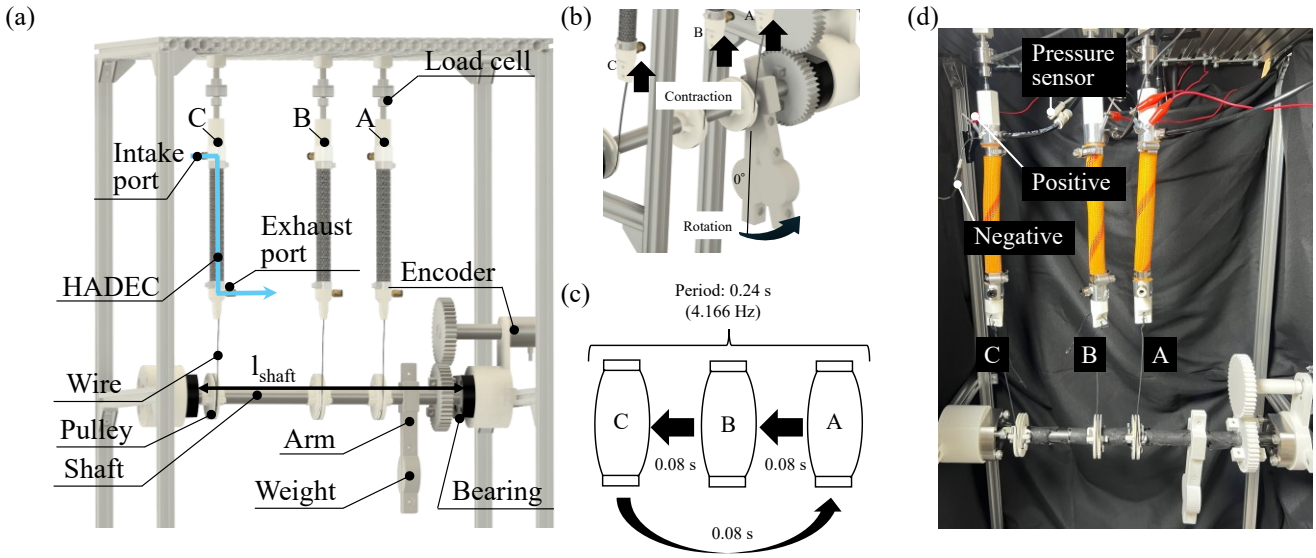

Fig. 3 Experimental Overview. (a) Overview of the experimental setup. (b) Close-up of the arm rotation mechanism. (c) Conceptual diagram of repeated actuation. (d) Photograph of the actual experimental setup.

Each torque component is given as follows.

$$\tau_{\mathrm{F}}(t) = F(t) \cdot r_{\mathrm{pulley}} \tag{7}$$

$$\tau_{\mathrm{weight}}(t) = -m_{\mathrm{weight}} \cdot g \cdot l_{\mathrm{weight}} \cdot \sin\theta\,(t) \tag{8}$$

$$\tau_{\mathrm{gravity}}(t) = -m_{\mathrm{arm}} \cdot g \cdot \frac{l_{\mathrm{arm}}}{2} \cdot \sin\theta\,(t) \tag{9}$$

$$\tau_{\mathrm{viscosity}}(t) = -c_{\mathrm{d}} \cdot {l_{\mathrm{g}}}^2 \cdot \dot{\theta} \tag{10}$$

$$\tau_{\mathrm{friction}}(t) = -\mu(m_{\mathrm{arm}}+m_{\mathrm{weight}}) \cdot g \cdot r_{\mathrm{shaft}} \cdot sign(\dot{\theta}) \tag{11}$$

The internal volume V(t) of the HADEC during contraction can be expressed as a function of the contraction displacement $x(t)$, which is derived from the relationship between the angular acceleration of the pulley and the linear acceleration of the wire: $\ddot{x} = r_{\mathrm{pulley}} \cdot \ddot{\theta}$.

$$V(t) = \frac{\pi {d_0}^2}{4\,sin^2\theta_0}\left(1 - \frac{L^2\,cos^2\theta_0}{{L_0}^2}\right)\left(L_0 - x(t)\right) \tag{12}$$

Based on the PAM model, the contraction force F(t) of each artificial muscle can be expressed using the strain ε (t) as follows [24][25].

$$F(t) = \frac{\pi d_0^2 P(t)}{4sin^2\theta_0}\{3(1-\varepsilon(t))^2\,cos^2\theta_0 - 1\} \tag{13}$$

The initial conditions were set as $\theta(0) = 0$ [rad], $\dot{\theta}(0) = 0$ [rad/s] The number of moles of gas inside the chamber, n(t), is defined based on two states: during combustion and after combustion. During combustion, the mole count increases linearly as the gas mixture burns, and is expressed as follows [21].

$$n(t) = n_0 \cdot \left(1 + \frac{rt}{t_{\mathrm{dme}}}\right) \quad (0 \le t \le t_{\mathrm{dme}}) \tag{14}$$

Although the actual combustion process is expected to exhibit nonlinear characteristics with respect to time, a linear increase in molar quantity was assumed during the short combustion duration for simplification in simulation.

After the combustion phase, it is assumed that the generated gas is gradually expelled from the artificial muscle. Accordingly, the number of moles n(t)n(t)n(t) is modeled to decay exponentially, as expressed by the following equation [26].

$$n(t+\Delta t) = n(t) \cdot exp\left(-\frac{dt}{\tau_{\mathrm{n}}}\right) \quad (t \ge t_{\mathrm{dme}}) \tag{15}$$

Here, τ_n is the time constant associated with the decay of the number of moles. The numerical simulation was performed using a custom MATLAB code employing the forward Euler method with a time step of $\Delta t = 5.0\times10^{-4}$ s. The initial conditions were set to $\theta(0) = 0$ rad and $\dot{\theta}(0) = 0$ rad/s, and the parameters were determined based on those listed in Table 1. During the combustion duration ($t_{\mathrm{dme}} = 0.003$ s), the molar amount increased linearly, and it was designed to decay exponentially with a leakage time constant of $\tau_n = 0.005$ s. The temperature was updated using an energy balance equation, the pressure was calculated from the ideal gas law, and the contraction force was evaluated using a McKibben-type model. The obtained force was converted into torque through a pulley, and the arm's equation of motion was numerically integrated while accounting for inertia, gravity, viscous, and frictional terms. The simulation was conducted under the same driving frequency and phase shift conditions as those used in the subsequent experiments.

C. Fluidic and Electrical Circuits for Actuator Integration

To generate steady-state force, a premixed gas of DME and air is continuously supplied from a tank and each of the three HADEC is ignited sequentially with phase offsets. This is achieved by periodically triggering ignition at the electrodes embedded in the end fittings of each actuator.

Fig. 2 (b) shows the fluidic and electrical circuit diagrams used in this experiment for the integrated HADEC system. The premixed gas is delivered from the tank to each HADEC unit via a speed controller and a check valve. The check valve prevents backflow during combustion within the actuator.

The exhaust ports remain open at all times, allowing both combustion gases and unreacted fuel to be discharged easily. Since the system operates without solenoid valves, it provides a fluidic circuit structure well suited for actuator integration. On the other hand, when integrating a large number of fluid-driven actuators such as McKibben artificial muscles, it is necessary to equip each actuator with its own solenoid valve. This configuration may result in a system that is impractically large and heavy. As a solution to these conventional issues, the proposed system—capable of actuation without using solenoid valves—offers a significant advantage for actuator integration.

In the electrical circuit, ignition coils are connected to the electrodes of each HADEC unit. Pulse signals are sent from a PC to MOSFETs, which switch the high voltage from the ignition coils to the electrodes. This enables each artificial muscle to be individually actuated through combustion.

IV. Experiment

A. Objective of the Experiment

In this experiment, we evaluate the generation of steady-state force by rotating an arm using three HADEC actuators. Specifically, we measure and assess the arm's angular displacement, the contraction force generated by each HADEC, and the internal pressure within the actuators. While the HADEC has the potential to support larger angles, the 10° to 25° range was selected in this study to establish a stable baseline for evaluating continuous force generation and to minimize variations arising from external mechanical factors.

B. Setup

The experimental apparatus used in this study is shown in Fig. 3(a) and (b). Measurements were performed using an encoder (OMRON, E6B2-CWZ6C), a miniature pressure sensor (PISCO, SEU11-01A), and a load cell (KYOWA, LUR-A-500NSA1).

Each HADEC actuator has a contraction section with a length of 114 mm and an inner diameter of 16 mm. Both end fittings are equipped with two ports for supplying and exhausting the premixed gas, and appropriate tube fittings are attached for this purpose. A pressure sensor is installed just upstream of the intake-side end fitting. The ignition electrodes are embedded within the upper supply-side end fitting and are connected to an ignition coil (KITACO, Type A), which generates high voltage to produce a spark discharge between the electrodes (see Fig. 1 (d)).

Gas flow is regulated using a speed controller (PISCO, JSMU6) and a flow meter (SMC, PFM750-C6-C). The diameters of both inlet and outlet ports are 5 mm.

The structure of the arm is also shown in Fig. 3 (b). When each of the three artificial muscles contracts, it pulls on a wire, which rotates the pulley, resulting in arm motion. In the experimental setup, the three HADEC units were not positioned equidistantly around the shaft, as spatial constraints and wiring considerations necessitated asymmetric placement. However, since the actuator force is transmitted via wires to a common pulley, and the torque contribution depends primarily on contraction force rather than spatial placement, the effect of actuator positioning on load imbalance was considered negligible. A 200 g weight is embedded inside the arm, and its vertical downward position is defined as 0°. The system is configured such that the HADEC actuators are in a state of equilibrium with the gravitational torque of the arm under these initial conditions. All measurements were conducted using this setup.

C. Method

The fluidic and electrical circuit diagrams are shown in Fig. 2 (b). In the experiment, a premixed gas of DME and air with a molar ratio of 7.0% is prefilled into a tank and continuously supplied to the HADEC actuators at a flow rate of 3–5 L/min, regulated by a speed controller and a flow meter. Although increasing the gas flow rate could potentially result in a larger arm rotation angle, the flow rate was set to 3–5 L/min in this study to focus on demonstrating the feasibility of generating steady-state force. Under these continuous supply conditions, each HADEC is ignited by a spark generated between electrodes via ignition coils, as illustrated in Fig. 2 (b). The ignition is triggered by pulse signals sent from a PC to MOSFETs at a frequency of 4.166 Hz (0.24 s phase interval) per actuator, corresponding to a combined actuation frequency of 12.5 Hz (0.08 s phase interval) for the entire arm. This frequency was selected based on simulation results that explored the actuation frequency required to maintain steady-state force generation using three HADEC units. It corresponds to a 0.24 s actuator cycle (with a 0.08 s phase interval between units), which allows sufficient time for combustion gases to be exhausted before the next ignition, thereby reducing the risk of misfires caused by combustion gases. The combustion of the gas mixture causes each HADEC to contract, which in turn rotates the arm. The combustion products and any unreacted gas are expelled through the exhaust-side end fittings. In this experiment, the three HADEC actuators were designated A, B, and C, as shown in Fig. 3 (d), and the system was evaluated for its ability to generate steady-state force.

V. Experimental Results and Discussion

The experimental results are shown in Fig. 4 and Fig. 5. Fig. 5 presents an enlarged view of the response during the 0.4–1.6 s interval following actuation. In both graphs, any negative fluctuations in force and pressure associated with spark-induced noise are plotted as zero for clarity. As shown in Fig. 4, when the three HADEC actuators were repeatedly ignited at a frequency of 4.166 Hz with phase differences, the arm was maintained within an angular range of approximately 10°–20° for about 1.5 seconds. The initial arm rotation behavior closely matched the simulation results. The time from the output command to the peak contraction force was 0.01 s, and the arm reached its peak angle at 0.19 s. These results confirm that a rapid rise in contraction force due to combustion was successfully achieved. Furthermore, although the arm angle exhibited oscillations due to alternating actuation of the HADEC units, it remained within

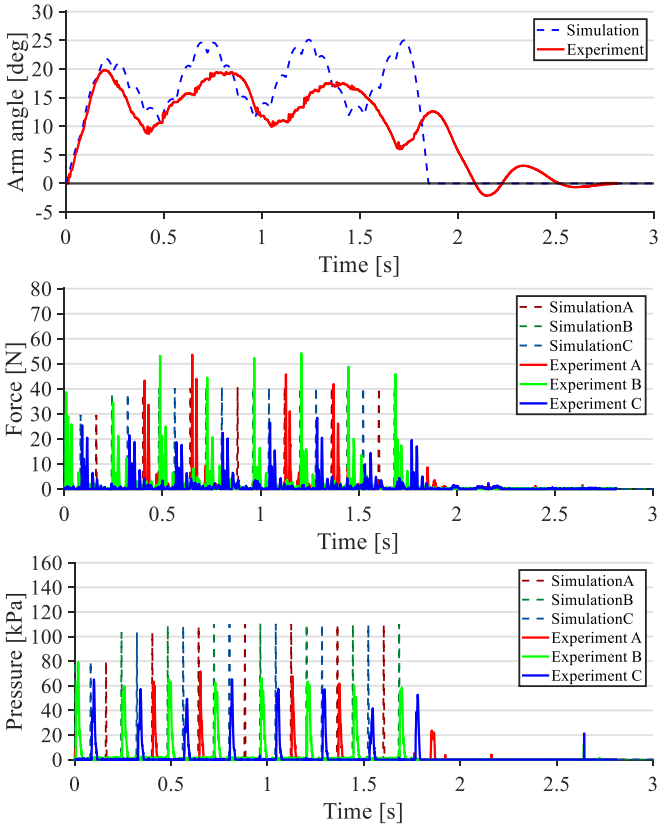

Fig. 4 Experimental Results. Time-series plots of angle, force, and internal pressure (from top to bottom).

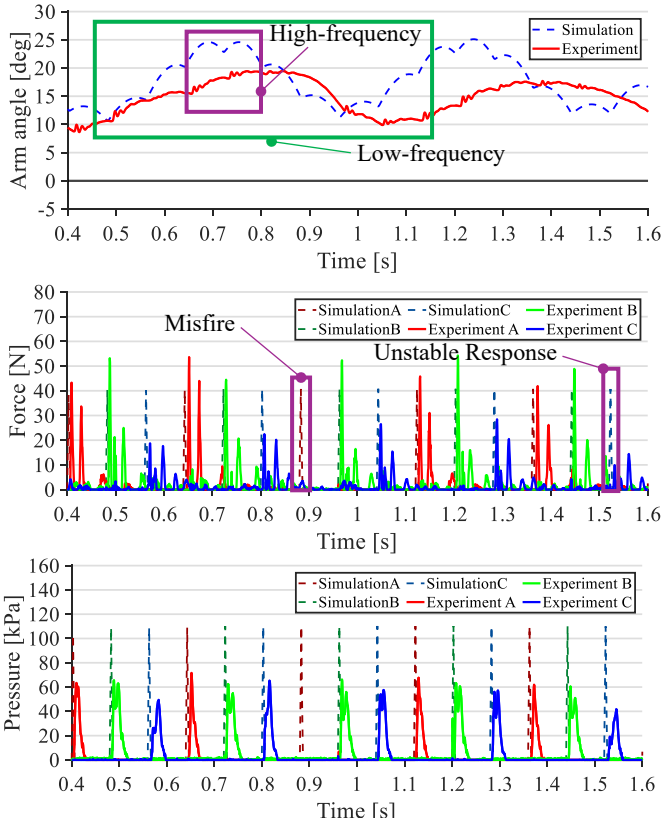

Fig. 5 Experimental Results (Enlarged View from 0.4 s to 1.6 s). Time-series plots of angle, force, and internal pressure (from top to bottom).

a bounded range, demonstrating that steady-state force generation was successfully realized.

Furthermore, analysis of the arm's behavior during steady-state operation revealed the presence of two distinct frequency components. The high-frequency component (e.g., the purple-highlighted region in the angle variation graph of Fig. 5) corresponds to the actuation frequency of the HADEC units, and matches the timing of the ignition control. The amplitude of this vibration was relatively small and showed good agreement with the theoretical model. In contrast, the lower-frequency component (e.g., the green-highlighted region in Fig. 5) is believed to originate from the dynamic characteristics of the entire arm system—specifically, the rotational response induced by actuator contraction, as well as oscillations affected by gravity and friction. While this low frequency behavior also exhibited qualitative agreement with the simulation, there remains room for improvement in achieving smoother output. For example, the high-frequency oscillations could be further attenuated by increasing the number of HADEC units or by increasing the actuation frequency. To suppress the low-frequency components, one potential approach is to configure antagonistic artificial muscles, similar to biological muscles, and introduce redundancy among actuators. This strategy could help stabilize arm motion. Additionally, introducing moderate damping or frictional elements where appropriate may promote vibration attenuation and improve the overall operational stability of the system.

On the other hand, the contraction force graphs in Fig. 5 reveal instances where ignition failed to occur properly, as indicated by the purple-highlighted regions in the force–time plots. Additionally, even in cases where combustion was successfully initiated, insufficient contraction force was observed, indicating variability in actuator performance. During these moments, the arm angle could not be maintained, resulting in discrepancies between the experimental results and the simulation. This issue is likely attributable to an insufficient spark gap between the electrodes, indicating the need for improvements in ignition rate. Additionally, differences in contraction force among the three HADEC units were observed. In particular, actuator C exhibited significantly lower output, limited to around 40 N, compared to the other two. The differences in contraction force among the three HADEC units are attributed not to actuator placement, but rather to physical variation in sleeve braiding angle, initial wire tension, or material inconsistencies. Given that all actuators apply force via the same pulley mechanism, spatial positioning is not expected to significantly influence load distribution or torque generation. This disparity is presumed to result from variations in the braiding angle of the sleeve, manufacturing inconsistencies in the rubber tube, and differences in the initial tension of the connecting wire. According to the internal pressure measurements shown in Fig. 5, all three HADEC actuators achieved comparable combustion pressures, suggesting that the fuel combustion amount was not a primary source of variation. However, the observed differences in output force indicate that individual

actuator characteristics and mechanical transmission factors had a substantial impact on the overall performance.

In the current simulation, the combustion duration was assumed to be 0.003 seconds. However, to construct a more accurate model based on the actual combustion process, it is necessary to obtain empirical data on the combustion rate during repeated ignition in future work. In addition, although HADEC actuators with an inner diameter of 16 mm were used in this study, future work will explore the development of smaller-diameter HADEC actuators. These will be used in parallel to drive the system, with the aim of creating wearable prototypes and mimicking the structure of biological muscles. A hybrid actuation approach that combines HADEC with conventional PAM is also under consideration. Unlike PAM, which require valve operations to control pressurization and depressurization, HADEC can operate without sealing the actuator, relying solely on ignition-based actuation. However, integrating a large number of PAMs introduces complexity due to the increased number of required valves. Therefore, the practicality of such a hybrid system must be carefully evaluated based on the intended application.

VI. CONCLUSION

In this study, we focused on the structure of biological muscles and demonstrated that steady-state contraction force can be achieved by repeatedly actuating three HADEC, which utilize the ignition of DME. The integrated actuation system successfully maintained an arm within a range of approximately 10° to 20° for about 1.5 seconds. The initial response closely matched the simulation results, confirming that the system can simultaneously achieve high responsiveness and steady output—an outcome that has been challenging with conventional PAM. However, variations in ignition timing and individual actuator performance led to output inconsistencies. Therefore, future work should aim to improve the ignition mechanism, suppress variations among actuators, and enhance output stability by miniaturizing the actuators and increasing the number of HADEC units.

These findings suggest that the integration of HADEC actuators offers a promising approach to realizing high-response and steady force generation—capabilities that are difficult to achieve with conventional PAM. Continued development is expected to further advance the practicality and stability of such systems.

Appendix

TABLE I Parameters in chapter III

Name			*Unit*
Universal gas constant	R	8.31	[*J/(mol·K)*]
Initial temperature	T_0	300	[*K*]
Atmospheric pressure	P_a	101300	[*Pa*]
Inner diameter of rubber tube	d_0	0.016	[*m*]
Initial length	L_0	0.14	[*m*]
Specific heat at constant volume	c_v	12.5	[*J/(mol·K)*]
Equivalent external heat capacity	C	0.3	[*J/K*]
Molar mass of DME	M	46	[*g/mol*]
Molar ratio	r	0.07	[-]
Heat of combustion of DME	Q_{DME}	28800	[*J/g*]
Braiding angle	θ_0	0.6981(=40°)	[*rad*]
Leakage time constant	τ_n	0.005	[*s*]
Mass of HADEC	m	0.2	[*kg*]
Spring constant of HADEC	k	1000	[*N/m*]
Viscous coefficient of HADEC	c	0.001	[*N·s/m*]
Combustion duration	t_{dme}	0.003	[*s*]
Injected molar amount	n	0.0009	[*mol*]
Thermal penetration depth	w	0.001	[*m*]
Thermal conductivity	λ	0.25	[-]
Surface area	S	0.007037	[m^2]
Initial volume	V_0	0.000028	[m^3]
Combustion energy	Q_{in}	106.07	[*J*]
Pulley radius	r_{pulley}	0.024	[*m*]
Mass of arm	m_{arm}	0.032	[*kg*]
Length of arm	l_{arm}	0.15	[*m*]
Mass of weight	m_{weight}	0.2	[*kg*]
Distance to weight	l_{weight}	0.05	[*m*]
Radius of weight	r_{weight}	0.025	[*m*]
Mass of pulley	m_{pulley}	0.2	[*kg*]
Mass of shaft	m_{shaft}	1.5	[*kg*]
Shaft radius	r_{shaft}	0.01	[*m*]
Gravitational acceleration	g	9.81	[m/s^2]
Kinetic friction coefficient	μ	0.0005	[*N·m/rad*]
Viscous torque coefficient	c_d	0.002	[*N·m·s/rad*]

ACKNOWLEDGMENT

THIS WORK WAS SUPPORTED BY JSPS KAKENHI GRANT NUMBER 25K21256 AND JST ACT-X GRANT NUMBER JPMJAX21K2.

REFERENCES

[1] J. Fras, Y. Noh, M. Macias, H. Wurdemann, and K. Althoefer, “Bio-inspired octopus robot based on novel soft fluidic actuator,” in Proc. IEEE Int. Conf. Robot. Automat., 2018, pp. 1583–1588.

[2] Y. Hotoda and K. Ito, “Octopus-like soft robot hand for handling vegetables and fruits,” in Proc. Int. Conf. Adv. Mechatronic Syst., 2023, pp. 13–18.

[3] R. Chen, X. Zhu, Z. Yuan, H. Pu, J. Luo, and Y. Sun, “A bioinspired single actuator-driven soft robot capable of multistrategy locomotion,” IEEE Trans. Robot., vol. 40, pp. 2149–2165, 2024.

[4] J. Tirado, J. Jørgensen, and A. Rafsanjani, “Earthworm-inspired multimodal soft actuators,” in Proc. IEEE Int. Conf. Soft Robot., 2023, pp. 1–6.

[5] D. D. K. Arachchige, D. M. Perera, S. Mallikarachchi, U. Huzaifa, I. Kanj, and I. S. Godage, “Soft steps: Exploring quadrupedal locomotion with modular soft robots,” IEEE Access, vol. 11, pp. 63136–63148, 2023.

[6] X. Ai, H. Yue, and W. D. Wang, “Crawling soft robot exploiting wheel-legs and multimodal locomotion for high terrestrial maneuverability,” IEEE Trans. Robot., vol. 39, no. 6, pp. 4230–4239, Dec. 2023.

[7] W. R. Johnson, S. J. Woodman, and R. Kramer-Bottiglio, “An electromagnetic soft robot that carries its own magnet,” in Proc. IEEE 5th Int. Conf. Soft Robot., 2022, pp. 761–766.

[8] E. Zhang and E. Zhang, "Omnimobile and Load Capable Pneumatic Soft Robot for Gas Distribution Pipeline Inspection," 2025 IEEE 8th International Conference on Soft Robotics (RoboSoft), Lausanne, Switzerland, 2025, pp. 1-6.

[9] Design of a Fully-Soft Lift-Assist Wearable Suit Powered by Flat Inflatable Artificial Muscles," in IEEE Robotics and Automation Letters, vol. 10, no. 5, pp. 4428-4435, May 2025.

[10] L. Campioni et al., "Preliminary Evaluation of a Soft Wearable Robot for Shoulder Movement Assistance," in IEEE Transactions on Medical Robotics and Bionics, vol. 7, no. 1, pp. 315-324.

[11] G. Andrikopoulos, G. Nikolakopoulos and S. Manesis, "A Survey on applications of Pneumatic Artificial Muscles," 2011 19th Mediterranean Conference on Control & Automation (MED), Corfu, Greece, 2011, pp. 1439-1446.

[12] M. A. Khan, S. Shaik, M. H. Tariq and T. Kamal, "McKibben Pneumatic Artificial Muscle Robot Actuators - A Review," 2023 International Conference on Robotics and Automation in Industry (ICRAI), Peshawar, Pakistan, 2023, pp. 1-6.

[13] Y. Liu, Y. Yang, Y. Peng, S. Zhong, N. Liu and H. Pu, "A Light Soft Manipulator With Continuously Controllable Stiffness Actuated by a Thin McKibben Pneumatic Artificial Muscle," in IEEE/ASME Transactions on Mechatronics, vol. 25, no. 4, pp. 1944-1952, Aug. 2020.

[14] T. Ito, K. Uchiyama and H. Tomori, "Development of an Endoskeletal-Type Leg Assistive Orthosis Using Pneumatic Rubber Artificial Muscles," IECON 2023- 49th Annual Conference of the IEEE Industrial Electronics Society, Singapore, Singapore, 2023, pp. 1-6 .

[15] Y. Peng, Y. Sakai, Y. Funabora, K. Yokoe, T. Aoyama and S. Doki, "Funabot-Sleeve: A Wearable Device Employing McKibben Artificial Muscles for Haptic Sensation in the Forearm," in IEEE Robotics and Automation Letters, vol. 10, no. 2, pp. 1944-1951, Feb. 2025.

[16] M. Liu and L. Hao, "Design and control of a robotic wrist joint actuated by the shape memory alloy actuator," 2021 IEEE 11th Annual International Conference on CYBER Technology in Automation, Control, and Intelligent Systems (CYBER), Jiaxing, China, 2021, pp. 225-229.

[17] A. Osorio Salazar, Y. Sugahara, D. Matsuura, and Y. Takeda, “Scalable output linear actuators, a novel design concept using shape memory alloy wires driven by fluid temperature,” Machines, vol. 9, no. 1, p. 14, 2021.

[18] M. Duduta, D. R. Clarke and R. J. Wood, "A high speed soft robot based on dielectric elastomer actuators," 2017 IEEE International Conference on Robotics and Automation (ICRA), Singapore, 2017, pp. 4346-4351.

[19] M. Kadokawa and C. Jiang, "Development of a Thin Dielectric Elastomer Actuator with 3DOFs," 2021 International Conference on Advanced Mechatronic Systems (ICAMechS), Tokyo, Japan, 2021, pp. 12-15.

[20] A. M. Okui, S. Iikawa, Y. Yamada and T. Nakamura, "1st prototype of a variable viscoelastic joint system with a clutch composed of pneumtic air muscle and magneto rheological brake," 2016 14th International Conference on Control, Automation, Robotics and Vision (ICARCV), Phuket, Thailand, 2016, pp. 1-6.

[21] K. Mori, K. Tsurumi, R. Sawahashi, R. Enjo, T. Nakamura and M. Okui, "HADEC - High-Response Artificial Muscle Actuator Using Dimethyl Ether Combustion," in IEEE Robotics and Automation Letters, vol. 10, no. 7, pp. 6952-6959, July 2025

[22] T. Kaoru, “Dimethyl ether (DME): A clean fuel/energy for the 21st century and the low carbon society,” Int. J. Energy Environ., vol. 10, pp. 248–252, 2016.

[23] C. J. Heckman and R. Enoka, "Motor Unit," Comprehensive Physiology, vol. 2, pp. 2629–2682, 2012 .

[24] C.-P. Chou and B. Hannaford, “Measurement and modeling of McKibben pneumatic artificial muscles,” IEEE Trans. Robot. Automat., vol. 12, no. 1, pp. 90–102, Feb. 1996.

[25] A. Nozaki and T. Noritsugu, “Finite element analysis of the motion of McKibben-type pneumatic rubber artificial muscles,” Int. J. Automat. Technol., vol. 8, no. 2, pp. 147–158, 2014.

[26] G. K. Costa, “Modelling air flow through pneumatic valves: A brief review with an experimental case study,” Eng, vol. 4, pp. 2601–2614, 2023.